Journal of
Manufacturing and Materials Processing

MDPI

Article

The Optimization of Severe Shot Peening Coverage for Enhanced Fatigue Performance of AISI 4140 Steel: A Combined Experimental and FE-Cell Approach

Mohsen Forouzanmehr [1,2], Kazem Reza Kashyzadeh [3], Reza Namdar [4], Hadi Salavati [1], Hossein Darijani [1] and Mahmoud Chizari [5,*]

[1] Department of Mechanical Engineering, Shahid Bahonar University of Kerman, Kerman 7616914111, Iran
[2] Coal Mining Training Center, University of Applied Science and Technology, Tehran 1599665111, Iran
[3] Department of Transport Equipment and Technology, Academy of Engineering, RUDN University, 6 Miklukho-Maklaya Street, Moscow 117198, Russia; reza-kashi-zade-ka@rudn.ru
[4] Academic Center for Education, Culture and Research (ACECR), Kerman 145997411, Iran
[5] School of Physics Engineering and Computer Science, University of Hertfordshire, Hatfield AL10 9AB, UK
* Correspondence: m.chizari@herts.ac.uk

Abstract

Shot peening is widely used to improve fatigue performance by introducing compressive residual stresses, but the influence of very high coverage levels on medium carbon steels such as AISI 4140 remains unclear. This work investigates conventional and severe shot peening at 100%, 400%, 1000%, and 1500% coverage under a fixed 18A Almen intensity, combining rotating-bending fatigue experiments with a finite element cell (FE-Cell) approach for residual stress quantification. Fatigue tests were conducted at stress amplitudes of 37 MPa, 40.5 MPa, and 44 MPa, supported by surface roughness, hardness, and fractographic characterization. The results show a strong coverage–stress interaction: at 37 MPa, severe shot peening at 1000% coverage yields the maximum fatigue life improvement, whereas at 44 MPa the optimum shifts to 400% coverage, and excessive coverage (1500%) produces over-peening, microcrack networks, and reduced life. FE-Cell simulations reveal that increasing coverage deepens and intensifies compressive residual stresses but also promotes stress redistribution at extreme coverage. The combined findings define an optimal processing window of 400–1000% coverage for AISI 4140, balancing deep compressive residual stresses with controlled surface integrity and providing practical guidelines for industrial severe shot peening of rotating components.

Keywords: shot peening; severe shot peening; AISI 4140 steel; fatigue life; residual stress; FE-Cell method; surface roughness; coverage optimization

Academic Editor: Steven Y. Liang

Received: 14 March 2026
Revised: 13 April 2026
Accepted: 16 April 2026
Published: 21 April 2026

1. Introduction

Fatigue failure represents one of the most critical degradation mechanisms in mechanical components subjected to cyclic loading, often culminating in catastrophic fracture at stress levels substantially below the material's yield strength [1]. This phenomenon arises from progressive damage accumulation during repeated loading cycles, eventually initiating and propagating cracks that compromise structural integrity. The fatigue life of engineering components is governed by an intricate interplay of mechanical, metallurgical, and environmental factors, encompassing grain size, yield strength, toughness, component geometry, surface condition, applied loading characteristics, and residual stress states [2].

AISI 4140 steel, recognized for its exceptional combination of high strength and toughness, finds widespread application in critical engineering systems, including gearboxes, transmission shafts, and aircraft landing gear components [3]. Nevertheless, the fatigue performance of this alloy under cyclic loading, particularly rotational bending conditions, presents opportunities for substantial enhancement through strategic surface modification techniques such as shot peening.

Shot peening constitutes a well-established surface treatment wherein controlled bombardment with spherical media induces beneficial compressive residual stresses and work-hardening effects that impede crack initiation and propagation [4,5]. Conventional shot peening, typically applied at coverage levels of 100–200%, has been extensively documented to improve fatigue resistance through the establishment of compressive residual stress fields [2,4,5]. However, the phenomenon of over-peening—wherein excessive coverage induces surface damage, stress relaxation, and accelerated crack initiation—limits the effectiveness of this approach [2,4,5]. Recent investigations have demonstrated that severe shot peening, extending coverage beyond conventional limits, offers potential for further fatigue enhancement through nanostructured surface layer formation, though the optimal coverage threshold remains material-specific and poorly defined for medium-carbon steels [6–8].

For shot-peened steel alloys, Karimbaev et al. [6] demonstrated that the fatigue behaviour of as-received specimens was improved by shot peening and further enhanced by combination with ultrasonic nanocrystal surface modification, with the combined treatment exhibiting superior fatigue life improvement. Farrahi et al. [4] established that larger shot sizes maximized fatigue life in spring steel under reversed torsion, while lower, harder shots proved superior for short-term applications, revealing that residual stresses and work hardening degrade cyclically with rates dependent on stress levels and deformation magnitude. Maleki et al. [7] investigated shot peening treatments across Almen intensities of 17 and 21 A and coverage ranging from 100% to 1500%, demonstrating that residual stress relaxation initiated at early loading stages and progressed gradually, with severe shot peening exhibiting lower relaxation rates than conventional treatment. In subsequent work, Maleki et al. [8] showed that increasing kinetic energy in AISI 1045 steel produced nanostructured surface layers with significant fatigue strength improvement, though coverage exceeding 1000% degraded performance through micro-damage accumulation. These studies collectively indicate that severe shot peening occupies a complex parameter space where benefits from deep compressive stresses and nano-structuring must be balanced against detrimental surface damage. Although severe shot peening may improve fatigue resistance by generating deeper compressive residual stresses and modifying the near-surface microstructure, excessive processing can also produce unfavourable effects, including increased surface roughness, initiation of microcracks, and accumulation of damage within the hardened layer. Prior work has shown that severe shot peening can trigger microstructural evolution together with redistribution of residual stress; in some cases, the resulting surface damage can offset the strengthening gains [9]. Therefore, the net benefit of severe shot peening depends critically on maintaining an optimal balance between the degree of plastic deformation and preservation of surface integrity.

Despite extensive research on shot peening coverage effects, critical knowledge gaps persist regarding high-coverage regimes beyond 400%, particularly for AISI 4140 steel under rotational bending fatigue. For this alloy, no studies have systematically explored extreme coverage levels of 1000–1500%, where severe plastic deformation could either enhance fatigue resistance through nanocrystalline layer formation or degrade it through surface spalling and microcracking. The establishment of comparable residual stress fields across varying coverage levels presents additional methodological challenges.

Forouzanmehr et al. [10] addressed this through a general methodology introducing the FE-Cell method for comparing residual stresses induced by ring indentation, punching, and shot peening, demonstrating that deeper compressive residual stress penetration constitutes a key factor for fatigue crack retardation in aluminum alloys. This technique was subsequently validated for punching processes using FE-path analysis [11]. However, three major deficiencies remain in the existing literature: no studies address AISI 4140 alloy fatigue response to systematic shot peening coverage variation under rotating bending conditions; the effects of high coverage levels of 400–1500% remain unexplored for this material; and no clear threshold has been established for over-peening in this alloy where beneficial effects transition to detrimental outcomes. Recent studies (2023–2025) have further confirmed the potential of severe shot peening for fatigue enhancement while emphasizing the need for coverage optimization to avoid over-peening degradation.

The present investigation addresses these gaps through a systematic evaluation of conventional and severe shot peening effects on AISI 4140 steel fatigue performance. This study applies shot peening at coverages of 100%, 400%, 1000%, and 1500% under fixed 18A Almen intensity, with fatigue testing conducted under rotating-bending conditions at controlled stress amplitudes. The research implements the FE-Cell methodology for comparative residual stress field analysis across coverage levels, complemented by comprehensive surface characterization encompassing roughness, hardness, and fractographic examination. The central aim of this work is to identify the optimal shot peening coverage range that maximizes fatigue life enhancement while avoiding over-peening degradation, thereby establishing processing guidelines for industrial application of severe shot peening to critical AISI 4140 components.

2. Experimental Procedures

2.1. Material and Specimen

In the present study, AISI 4140 or 42CrMo4 steel was selected as the specimens. This steel alloy is employed widely for engineering components due to its high strength, excellent toughness, wear resistance, and fatigue strength. The chemical composition of AISI 4140 steel is mentioned in Table 1.

Table 1. Nominal chemical composition of AISI 4140 steel [12].

Element	C	Si	Mn	P	S	Cr	Mo	Fe
Composition (wt%)	0.38–0.43	0.15–0.35	0.75–1.00	≤0.035	≤0.040	0.80–1.10	0.15–0.25	Balance

Based on the obtained chemical properties and comparison of the compositional analysis results, the mechanical properties of this material were determined through tensile testing and are reported in Table 2.

Table 2. Mechanical properties of annealed AISI 4140 steel [13] determined through tensile testing.

Yield Strength (MPa)	Ultimate Strength (MPa)	Young's Modulus (GPa)	Density Kg/m^3	Poisson's Ratio
458	610	210	7840	0.3

To fabricate the fatigue specimens, firstly, AISI 4140 alloy steel was annealed at 872 °C, followed by slowly cooling in the furnace. The specimen geometry was designed in compliance with ISO 1143 [14], which provides dimensional proportionality rules for cylindrical test specimens. As the bending fatigue test was the primary focus, the specimen dimensions

were derived accordingly. Figure 1 illustrates the polished specimen surface with standardized dimensions, and Figure 2 shows the test matrix, which included 12 specimens: three specimens as-received and three for each level of SP, 100% coverage, and severe shot peening conditions (400%, 1000%, and 1500% coverage).

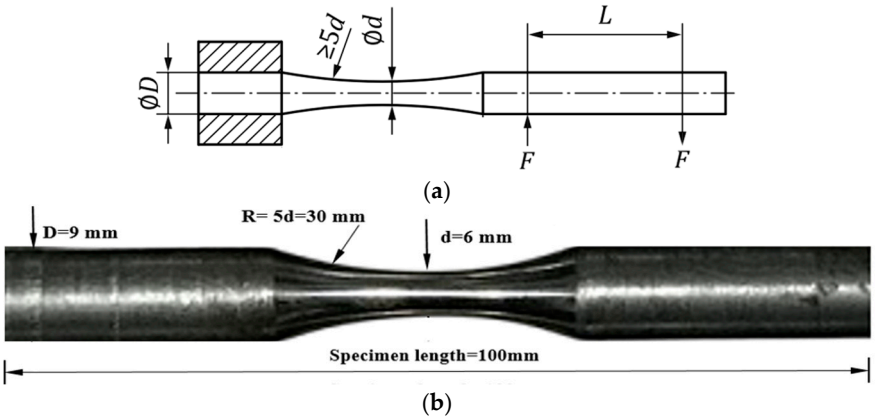

Figure 1. Rotating bending fatigue specimen geometry per ISO 1143:2021: (**a**) polished as-received specimen showing gauge section and fillet radii; (**b**) critical dimensions—gauge diameter 6 mm, gauge length 30 mm, fillet radius 60 mm, overall length 120 mm; surface finish profile with arithmetic mean roughness $\leq$ 0.2 µm prior to shot peening.

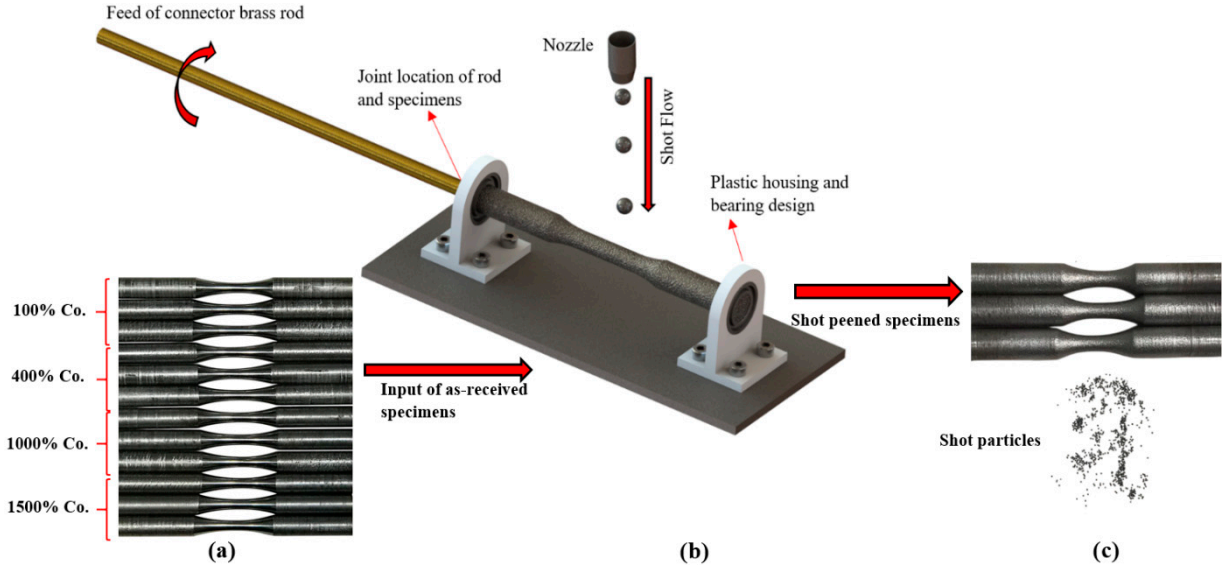

Figure 2. Shot peening experimental setup and specimen preparation: (**a**) as-received AISI 4140 specimens with mirror-finish surface prior to treatment; (**b**) rotational shot peening apparatus with specimen fixture, brass drive shaft, and S230 steel shot delivery system—nozzle diameter 6.335 mm, standoff distance 120 mm, impact angle 90°; (**c**) shot-peened specimens exhibiting matte surface finish with complete circumferential coverage achieved through controlled rotation.

2.2. Shot Peening Treatment

Different SP treatments, considering 18A Almen intensity and coverages, were applied to the specimens using air blast shot peening (ABSP). SAE J443 [15] was used for the SP procedure. The treatments were carried out with standard S230 steel shots [16] with an average hardness of 50 HRC, a diameter of 0.6 mm, impact angle of 90°, nozzle diameter of 6.335 mm, and nozzle distance of 12 cm. A manual drill was used to hold and rotate the brass connector shaft. The prepared specimens are shown in Figure 2a. As demonstrated in Figure 2b, a fixture included a plastic housing with a bearing type of AFBMA 12.1.4.1 [17]

and a base plate was implemented for the experimental setup. As shown in Figure 2b, a brass rod connection with a length of 300 mm was used to control rotation. Shot-peened specimens with the shot particles are shown in Figure 2c.

In the fatigue testing of rotational specimens, since the shot peening media does not impact the entire surface, only one-fourth of the target area is covered under normal nozzle alignment, as shown in Figure 3. Accordingly, a manually controlled motor with adjustable speed was employed. Given that the required exposure time for flat specimens under perpendicular impact is approximately 11 s for 100% coverage [18], and the minimum rotational speed of the drill is 10 RPM, and the specimen completes roughly two rotations during this time period. Based on a two-dimensional sector analysis and considering the shot-peened zone length, only one-quarter of the surface receives peening coverage as $\delta S = r.\delta\varphi.l$, where δS is the arc of curvature, $\delta\varphi$ is the limited arc angle of the sector, l is the length of the specimen. To achieve the full coverage of SP, to fully cover the surface of shot peening, the angle must be increased by four times $\delta\varphi = 4 \times 90$. To precisely determine the number of rotations, a reference mark was placed on the output shaft of the peening chamber, and the rotations were accurately counted. Therefore, higher coverage levels can be achieved by proportionally increasing the exposure time and rotation count. For instance, 400% coverage would require four rotations.

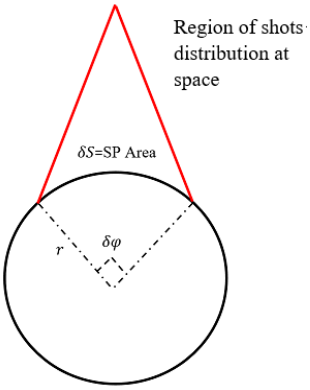

Figure 3. Rotational shot peening coverage principle: sector analysis showing limited arc exposure ($\delta\varphi$ = 90°) under a stationary nozzle, yielding 25% nominal coverage per rotation, versus full circumferential coverage achieved through four-fold angle multiplication (4 × 90° = 360°) with synchronized specimen rotation and shot delivery timing.

2.3. Fatigue Test, Surface Roughness, and Hardness Measurement

To survey the fatigue behaviour of samples, the rotating bending fatigue test was used. The applied stress amplitude is estimated as [19]:

$$\sigma_a = \frac{32M}{\pi d^3} \quad (1)$$

where $M = \alpha LW$ is the bending moment (N·m), d is the minimum cross-section of specimen (6 mm), W is the applied mass (kg), L is the distance from stress-section to loading point (200 mm), and α is the stress concentration factor (1.08). All tests are conducted at a stress ratio according to previous publication [20]. The loading process was performed by applying masses of 320 g, 350 g, and 380 g under stress-controlled conditions, corresponding to nominal stress amplitudes of 37 MPa, 40.5 MPa, and 44 MPa, respectively. All tests were conducted at a stress ratio of $R = -1$ and a frequency of 50 Hz at ambient temperature (23 ± 2 °C) according to ASTM E468-90 [20]. Three specimens were tested per condition to ensure statistical reliability.

To classify the specimens, untreated samples were designated as Class A, while shot-peened categories were classified by coverage level as Class B (100%), Class C (400%), and Class D (1000% and 1500%). A consistent stress level was assigned to each specimen group, with four coverage levels evaluated: 100%, 400%, 1000%, and 1500%.

Surface properties, including roughness and hardness, play a critical role in determining the performance of engineering components. This study examines the correlation between surface roughness parameters (R_a, R_q, R_t) and shot peening coverage. Roughness parameters were measured using a Mahr Pocket Surf PS1 Portable Surface Roughness Tester [21] according to ISO 4287 [22], with a cutoff length of 0.8 mm and evaluation length of 4 mm. Three measurements were taken at different locations on each specimen and averaged to obtain representative values.

To investigate the effects of severe shot peening on microhardness, hardness testing was performed using a Q30 hardness tester, Qness GmbH Co., Golling an der Salzach, Austria [23]. A Vickers indenter was applied with a 10 kgf load for a 7 s dwell time in accordance with ASTM E92-17 [24]. Indentations were made on the shot-peened surface and in the core region at 0.5 mm depth to determine surface and core hardness values, respectively. Five indentations per location were performed and averaged to ensure measurement reliability.

2.4. FE-Cell Method for Residual Stress Field Comparison

This section introduces the FE-Cell methodology [10,11] for comparing residual stress distributions in curved specimens subjected to shot peening. Figure 4a presents a schematic of the arbitrary domain of residual stress distribution (DRSD) in the curvature of a rotational bending fatigue specimen. To establish a framework for actual residual stress measurement, a representative cell with dimensions $a \times a \times h_c$ is defined within the treated region. The meshed cell, separated from the full structure for localized analysis, is shown in Figure 4b.

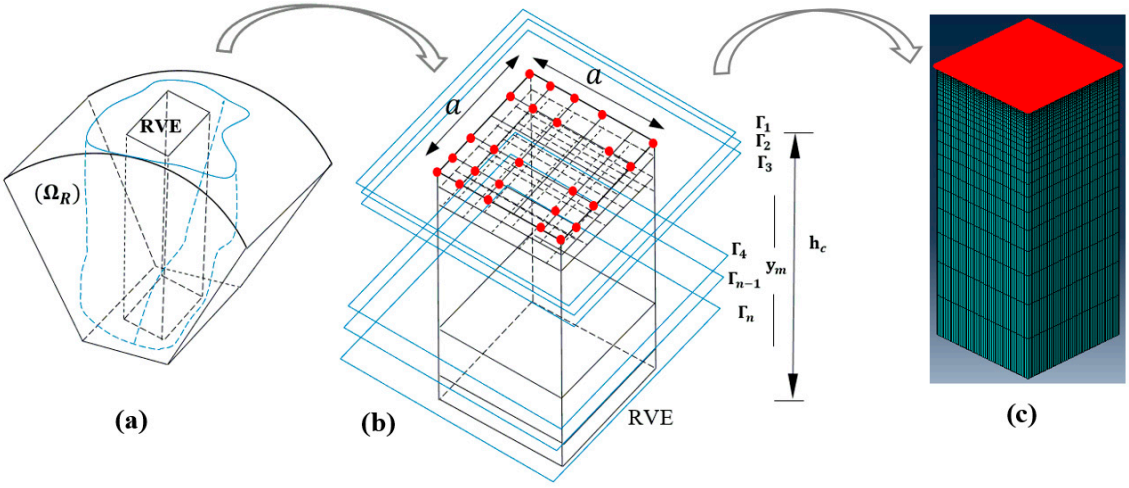

Figure 4. FE-Cell methodology for residual stress extraction in curved specimens: (**a**) arbitrary domain of residual stress distribution (DRSD) Ω-R on rotational bending fatigue specimen curvature; (**b**) representative volume element with nodal layers Γ_k for mean stress calculation at discrete depths y_m; (**c**) fully meshed cell ($1 \times 1 \times h_c$ mm^3) with C3D8R hexahedral elements in impact zone and boundary conditions—full constraint at substrate base, symmetry about midplane.

According to Figure 4b, mean residual stress profiles are calculated for each nodal element N_i (indicated as red points) on the Γ_k layers within the representative volume. The residual stress as a function of distance y from the surface is obtained using:

$$\sigma_{\Gamma_n}^{RS-x}(y_m) = \sigma_{\Gamma_n}^{ave}(y_m) = \frac{\sum \sigma_x^i}{\sum N_i} (\mathrm{n} = 1, 2, \ldots, \mathrm{p}) \quad (2)$$

where $\sigma_{\Gamma_n}^{RS-x}(y)$ is the residual stress field on the n^{th} layer, $\sigma_{\Gamma_n}^{ave}(y)$ is the mean stress component at nodal points on the k^{th} layer, σ_x^i is the stress component of the i^{th} nodal element (N_i), and y_m is the discretized cell height defined by Γ_k planes ($0 \leq y_m \leq h_c$). The residual stress at the surface (Γ_1, $y_m = 0$) is therefore:

$$\sigma_{\Gamma_1}^{RRS-x}(0) = \frac{\sum \sigma_x^i}{\sum N_i} \quad (3)$$

where $\sum N_i$ and $\sum \sigma_x^i$ represent the total number of nodal elements and the sum of their stress components, respectively. Local residual stress distributions are similarly reported for Γ_1, Γ_2, Γ_3 and Γ_k planes at increasing depths. By calculating residual stresses on these planes and plotting versus depth, the complete residual stress profile is obtained.

For numerical validation, the steel alloy is modelled as isotropic and homogeneous based on its mechanical properties and geometry [2,25]. The Johnson-Cook constitutive model [24] characterizes the elastic-plastic behaviour of the shot peening target. A representative volume element (RVE) Ω_R is defined on the residual stress field (Figure 4a). A meshed cell with dimensions $1 \times 1 \times h_c$ mm^3 is generated as the impact area (Figure 4c) to calculate residual stresses, extracted from a larger target domain of $1 \times 1 \times h_c$ mm^3. The cell height is set to 50 mm for validation studies and 30 mm for the present residual stress simulations. Although the specimen surface is curved and some shot impacts occur at oblique angles, the present FE model adopts a normal-impact assumption for the representative surface region. This simplification is intended to capture the dominant near-surface deformation and residual-stress response of the shot-peened zone. The resulting residual-stress field should therefore be interpreted as an averaged representation of the treated surface rather than a point-wise description of all impact angles. Consequently, the model is suitable for comparing the relative influence of coverage levels, while a small deviation from the real curved-surface response may remain due to oblique-impact effects.

2.5. Numerical Simulation of Random Shot Peening

The actual shot peening process, incorporating random shot distributions, was simulated using finite element models in ABAQUS/Explicit. Because the present study considers a rotational cylindrical specimen, the FE model assumes normal impact in the locally exposed region directly facing the nozzle, which represents the dominant peening condition in the central treated zone. This assumption captures the principal residual-stress development associated with the main impact direction. However, surface regions located away from the nozzle axis may experience oblique impact; therefore, the predicted residual-stress distribution should be regarded as an averaged representation of the near-surface peening effect rather than a pointwise exact reproduction of the entire curved surface. The associated deviation is expected to be minor in the directly impacted region and more pronounced near the peripheral zones of the treated area. Validation was performed for AISI 1050 steel at coverage levels of 100% and 1500% [18], followed by comprehensive simulations for AISI 4140 at 100%, 400%, 1000%, and 1500% coverage, all at a fixed 18A Almen intensity. The impact velocity of S230 shots was set to 70 m/s, calibrated against Almen intensity measurements [10].

The elastoplastic behaviour of the target material was characterized using the Johnson-Cook constitutive model with kinematic hardening [25,26]. A representative volume element (50 mm depth $\times$ 1 mm^2 surface area) was discretized using C3D8R reduced-integration hexahedral elements in the peening zone and C3D4 tetrahedral elements elsewhere [27]. A path of interest was defined along the cell centre in the Cartesian coordinate system for displacement analysis. Mesh convergence studies verified solution independence at dimple diameters of 24.28 μm for AISI 1050 (Figure 5) and 30.14 μm for AISI 4140, with a cubic element size of 20 μm adopted for both cases.

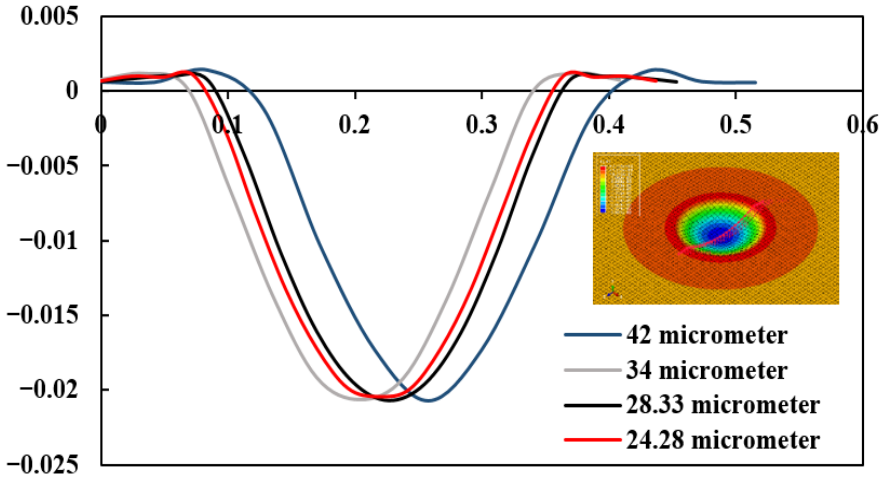

Figure 5. Mesh convergence verification for shot peening simulation, showing single-shot dimple diameters of 24.28 μm (AISI 1050) and 30.14 μm (AISI 4140) used for element size selection, with convergence demonstrating solution independence at 20 μm cubic element size—residual stress variation <5% with further refinement.

Boundary conditions enforced full constraint at the substrate base and symmetry about the midplane, with all rotational and translational movements of shot reference points restricted except in the y-direction. The model employed 64 shots (N) to achieve 100% nominal coverage, corresponding to 98% actual coverage per SAE J2277 [28].

Shot peening coverage was quantified using the approach of Kirk and Abyaneh [29], wherein randomly distributed shots impact the component surface within a defined area. Coverage ($Co\%$) is defined as the ratio of total indent area to target area A_r [27]:

$$Co\% = 100\left[1 - e^{-A_r}\right],\ \mathrm{A_r} = \frac{\mathrm{n} \times \pi\left(\frac{\mathrm{d}}{2}\right)^2}{\mathrm{A}} \tag{4}$$

where n is the number of shots applied to the target, A is the total treated surface area, d is the shot diameter, and $\pi(\frac{d}{2})^2$ is the indent area per shot. Substituting 98% actual coverage yields $A_r \approx 3.9$. For AISI 1050, this requires $N \approx 199$ shots for 100% actual coverage, while AISI 4140 requires $N \approx 504$ shots due to differing material properties. Higher coverages are achieved by multiplying the shot count by the coverage factor; for example, 1500% coverage requires $199 \times 15 = 2985$ shots for AISI 1050 validation.

Random shot locations were generated using a pseudo-random number algorithm [30]:

$$\begin{aligned} x &= -a/2 + a \times rand(0,1) \\ y &= -b/2 + b \times rand(0,1) \\ z &= 0.05 + \tfrac{d}{2} + (N-1) \times v \times \Delta t \end{aligned} \tag{5}$$

where a, b and are the peening area dimensions, d is the shot diameter, N is the shot number, v is the shot velocity, and $rand(0,1)$ generates pseudorandom numbers in $[0, 1]$. Shot positions were validated by ensuring minimum centre-to-centre distances S between hemispheres:

$$S = \sqrt{(x_i - x_j)^2 (y_i - y_j)^2 (z_i - z_j)^2} \tag{6}$$

The random shot assembly procedure is illustrated in Figure 6.

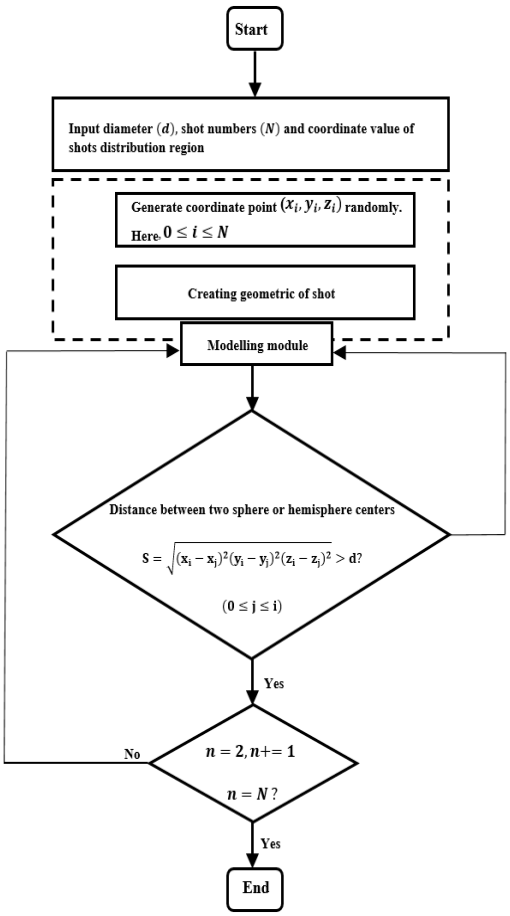

Figure 6. Random shot assembly algorithm for FE simulation: pseudo-random number generation for shot centre coordinates (x, y, z) with minimum centre-to-centre distance validation to prevent geometric overlap, iterative assembly until target shot count N is achieved for specified coverage percentage.

A Python script implemented this algorithm to generate shot distributions; Figure 7 illustrates the random shot pattern on the target surface for 1500% coverage. Dynamic shot motion and impact patterns were simulated over a 3 s interval, ensuring complete shot impact and rebound from the target surface.

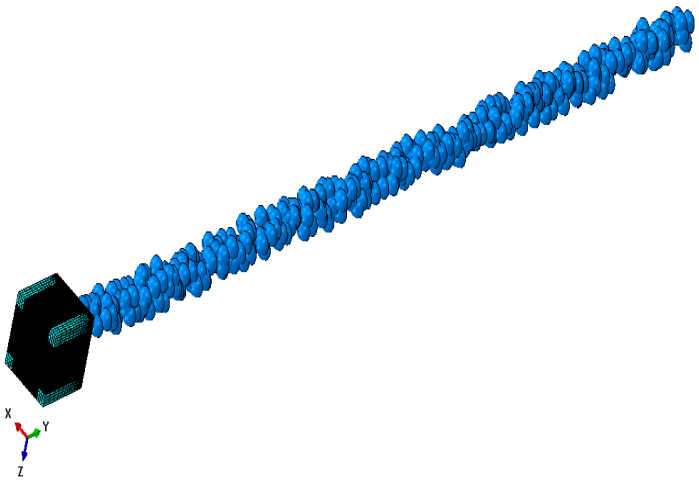

Figure 7. Random shot distribution on target surface for 1500% coverage simulation: 7560 S230 steel shots (diameter 0.6 mm) positioned via pseudo-random algorithm with minimum centre-to-centre distance constraint, achieving >98% surface coverage with stochastic impact pattern over 3 s simulation interval.

Table 3 summarizes shot parameters for model validation (AISI 1050, 100%, and 1500% coverage) and the present study (AISI 4140, 100%, 400%, 1000%, and 1500% coverage), including crater diameter, impact velocity, Almen intensity, and randomized shot counts.

Table 3. Shot parameters for FE model validation (AISI 1050) [15] and the present study (AISI 4140). Dimple diameters were determined through mesh convergence studies (Figure 5). Shot numbers were calculated using Equation (4) for 98% actual coverage.

Material	Coverage (%)	Shot Type	Shot Diameter (mm)	Dimple Diameter (μm)	Almen Intensity	Randomized Shot Numbers
AISI 1050 [18]	100	S230 Steel	0.6	24.28	18 A	199
AISI 1050 [18]	1500	S230 Steel	0.6	24.28	18 A	2985
AISI 4140 (Present Study)	100	S230 Steel	0.6	30.14	18 A	504
AISI 4140 (Present Study)	400	S230 Steel	0.6	30.14	18 A	2016
AISI 4140 (Present Study)	1000	S230 Steel	0.6	30.14	18 A	5040
AISI 4140 (Present Study)	1500	S230 Steel	0.6	30.14	18 A	7560

The present FE model adopts several simplifying assumptions that may influence the accuracy of residual stress predictions. The material is modelled as isotropic and homogeneous, neglecting potential microstructural gradients or anisotropic effects that may develop during severe plastic deformation. The Johnson–Cook constitutive model effectively captures strain-rate-dependent plastic flow under dynamic shot impacts but does not account for strain-induced phase transformations, dynamic recrystallization, or thermal softening that may occur at extreme coverage levels. These simplifications are standard in shot peening simulations but may lead to underestimation of near-surface work hardening saturation and slight overestimation of maximum compressive stress magnitudes. Despite these limitations, the relative trends in coverage-dependent residual stress evolution and depth profiles remain physically consistent with experimental fatigue performance.

3. Results and Discussion

Table 3 presents a systematic evaluation of shot peening effects across four coverage levels (100%, 400%, 1000%, and 1500%), with specimens categorized into Classes A–D based on applied stress levels. Fatigue performance was quantified through stress-controlled testing with cycle counts recorded for each condition. All fatigue life measurements were normalized against untreated (as-received) baseline specimens. The improvement ratio was calculated as:

$$\mathrm{IR} = \left(\frac{N_{SP} - N_{AR}}{N_{AR}}\right) \times 100\% \quad (7)$$

where N_{SP} is the fatigue life for a specific shot peening coverage, and N_{AR} is the fatigue life of as-received specimens. Class A specimens (37 MPa) demonstrated exceptional life improvement, achieving 797% enhancement at optimal 1000% coverage. Class B specimens (40.5 MPa) showed 538% improvement at optimal 1500% coverage, while Class C specimens (44 MPa) exhibited 405% enhancement at optimal 400% coverage. Beyond these optimal thresholds, excessive coverage induced surface microcrack nucleation and reduced fatigue performance: 33% life reduction at 1500% coverage under 37 MPa (Class A) and 15% decrease at 1500% coverage versus 400% under 44 MPa (Class C).

Detailed fatigue life data and improvement ratios are presented in Table 4, with Basquin fatigue parameters following in Table 5.

Table 4. Experimental fatigue life (Nf) by coverage and stress level (mean ± SD, n = 3).

Stress (MPa)	Condition	Cycles (N); (Mean ± SD)	Improvement vs. AR	Notes
37.0 (class A)	**As-received**	**30,322 ± 1820**	**Base**	
37.0 (A1)	SP-100%	51,220 ± 2840	+69%	
37.0 (A2)	SP-400%	110,022 ± 6060	+263%	
37.0 (A3)	SP-1000%	271,907 ± 14,970	+797%	Optimal
37.0 (A4)	SP-1500%	182,220 ± 10,050	+501%	Over-peening (−33%)
40.5 (class B)	**As-received**	**26,321 ± 1580**	**Base**	
40.5 (B1)	SP-100%	31,196 ± 1720	+19%	
40.5 (B2)	SP-400%	98,420 ± 5420	+274%	
40.5 (B3)	SP-1000%	95,429 ± 5260	+263%	
40.5 (B4)	SP-1500%	167,920 ± 9260	+538%	Optimal
44.0 (class C)	**As-received**	**19,120 ± 1150**	**Base**	
44.0 (C1)	SP-100%	28,300 ± 1560	+48%	
44.0 (C2)	SP-400%	96,522 ± 5320	+405%	Optimal
44.0 (C3)	SP-1000%	90,336 ± 4980	+372%	
44.0 (C4)	SP-1500%	82,120 ± 4530	+329%	Over-peening (−15%)

Table 5. Basquin fatigue parameters by shot peening coverage.

Coverage (%)	Fatigue Strength Coefficient $\sigma_f^{'}$ (MPa)	Fatigue Exponent, b	R^2
As-received	985.6	−0.105	0.978
100	1120.3	−0.092	0.985
400	1325.7	−0.087	0.991
1000	1580.2	−0.081	0.994
1500	1425.4	−0.084	0.989

All fatigue life values represent the mean ± one standard deviation from three replicate specimens per condition. Coefficients of variation ranged from 5.2% to 6.8% across all coverage levels, confirming adequate statistical repeatability for identifying coverage-dependent fatigue trends and optimal processing parameters. Despite the presence of experimental scatter, the relatively low coefficients of variation (5.2–6.8%) indicate good repeatability of the fatigue tests. Therefore, the use of mean values provides a reliable basis for regression, and the extracted Basquin parameters remain representative of the overall fatigue behaviour.

Basquin's relation (Equation (8)) was employed to characterize the stress-life behaviour and determine fatigue parameters for each coverage level:

$$\sigma_a = \sigma_f' \left(2N_f\right)^b \quad (8)$$

where σ_a is the stress amplitude (MPa), σ'_f is the fatigue strength coefficient (MPa), N_f is the number of cycles to failure, and b is the fatigue strength exponent. The Basquin parameters were determined by nonlinear regression fitting of experimental data for each coverage level, with coefficient of determination (R^2) values exceeding 0.97 for all fits (Table 5).

Basquin parameters were determined from the mean fatigue life values given in Table 4. Experimental scatter is represented separately through standard deviation and error bars and was not directly incorporated into the regression procedure. Analysis of Basquin parameters reveals that the fatigue strength coefficient peaks at 1000% coverage (1580.2 MPa), indicating superior fatigue resistance for this condition compared to other treatments. The fatigue strength exponent shows fewer negative values (closer to zero) at higher coverages, consistent with increased fatigue life in the high-cycle regime. The high values (>0.98) validate the goodness of fit for all coverage conditions.

The optimal coverage of 1000% at a 37 MPa stress level, achieving 797% fatigue life improvement, is supported by the maximum fatigue strength coefficient. At higher stress levels (44 MPa), the optimal coverage shifts to 400%, as excessive coverage induces surface damage that outweighs the benefits of deeper compressive stresses. The 1500% coverage shows a reduction compared to 1000%, confirming over-peening degradation despite deeper residual stress penetration.

The S-N diagram presented in Figure 8a validates the Basquin equation fit, with all curves achieving high coefficients of determination ($R^2 > 0.98$). Fatigue life peaks at 1000% coverage under 37 MPa (271,907 cycles, +797% improvement), demonstrating the benefits of severe shot peening under low-stress conditions. The 3D bar chart (Figure 8b) illustrates the coverage optimization landscape, showing that increasing stress level reduces life cycles at constant coverage. At higher stresses (44 MPa), 400% coverage performs optimally (96,522 cycles, +405%), indicating that excessive coverage induces surface damage under heavy loading, consistent with over-peening behaviour. Beyond optimal coverage (1500% at 37 MPa), life decreases by 33% due to microcrack formation, visible as the downward trend in the S-N curve at extreme coverage levels.

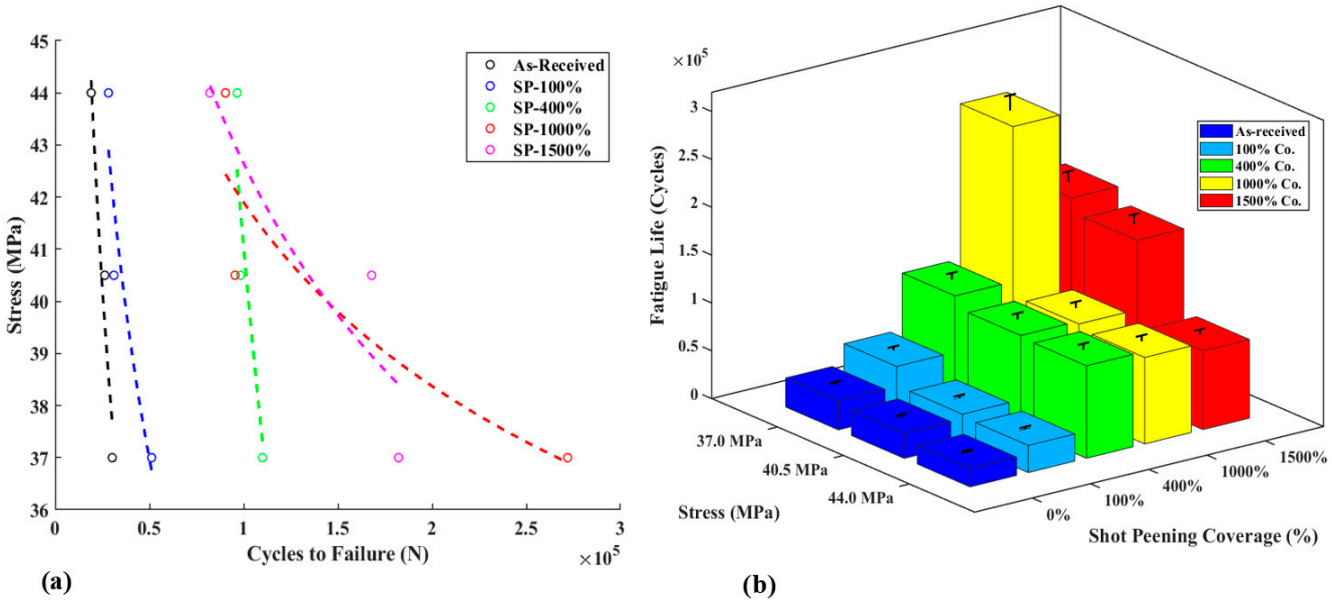

Figure 8. Fatigue performance characterization: (**a**) S-N curves for as-received and shot-peened specimens at varying coverage levels and stress amplitudes, with Basquin equation fits ($R^2 > 0.98$); (**b**) 3D coverage optimization landscape showing fatigue life as a function of shot peening coverage and applied stress, with optimal regions highlighted (error bars: mean ± SD, n = 3).

The surface coverage has a vital role, considering Almen intensity as a fixed parameter, in increasing surface roughness. The surface roughness parameter Ra rises after CSP and SSP [6]. However, more than 500% the variation in surface roughness is reached by a horizontal line in surfaces, and brief changes can be observed up to 1000% in a flat surface [7]. The surveys showed that the roughness parameter is more effective for fatigue life in LFC; however, residual stress is the key factor influencing HCF most [7]. The average of three lines of the treated surface is measured as a roughness parameter. The surface roughness parameters (R_a, R_q, and R_t) exhibit a consistent increase in these amounts by increasing the SP coverage. The as-received specimen shows minimal roughness (R_a = 0.2 µm, R_t = 1.5 µm). After treatment, R_a increases about 30 times (6.15 µm at 1500), while R_t surges to 41.2 µm, indicating deep surface irregularities. The rise in R_q (root mean square roughness) [2] from 0.25 µm to 7.5 µm suggests the development of pronounced peaks and valleys, likely due to increasing SP coverage. The influence of shot peening coverage on surface roughness is presented in Table 6.

Table 6. Surface roughness parameters of as-received and shot-peened specimens.

Specimen	R_a (µm)	R_q (µm)	R_t (µm)
As-received	0.20	0.25	1.50
100% coverage	2.97	3.74	22.60
400% coverage	4.37	5.52	31.00
1000% coverage	5.82	7.07	38.33
1500% coverage	6.15	7.50	41.20

Surface coverage significantly influences roughness development at fixed Almen intensity, with parameters R_a, R_q, and R_t increasing systematically with shot peening coverage [6]. Previous studies indicate that roughness variation plateaus beyond 500% coverage for flat surfaces, with marginal changes observed up to 1000% [7]. While roughness parameters predominantly affect low-cycle fatigue life, residual stress governs high-cycle fatigue behaviour [7].

The as-received specimen exhibits minimal roughness (R_a = 0.2 µm, R_t = 1.5 µm). After shot peening, R_a increases approximately 30-fold to 6.15 µm at 1500% coverage, while R_t surges to 41.20 µm, indicating substantial surface irregularity development. The rise in R_a from 0.25 µm to 7.50 µm reflects pronounced peak-and-valley formation due to cumulative shot impacts. Notably, the increment from 1000% to 1500% coverage is modest (5.8% for R_a, 6.1% for R_q), suggesting saturation of roughness generation as overlap density exceeds 50%.

Figure 9 illustrates the microstructural evolution of surface morphology under varying shot peening coverage levels. At 100% coverage (Figure 9a), relatively uniform peaks and valleys are observed with elongated surface microcracks and visible inclusion particles. Due to the random nature of shot peening, localized overlap zones develop at regions receiving multiple impacts, where adjacent dimple intersections occur. At this low coverage, such overlap phenomena remain limited.

At 400% coverage (Figure 9b), initial elongated microcracks are progressively obliterated through repeated plastic deformation, though new branched microcracks nucleate at refined scales. The overlap fraction rises to 25–30% of surface area as dimple intersections multiply, correlating with increased roughness (R_a from 2.97 µm to 4.37 µm). At 1000% coverage (Figure 9c), the transition to severe shot peening becomes evident: dimple depths intensify due to cumulative multi-impact deformation, overlap density surges to 45–50%,

and surface roughness increases to $R_a = 5.82$ µm. Notably, microcrack morphology shifts from micro-scale features to nano-scale bifurcated networks (<1 µm).

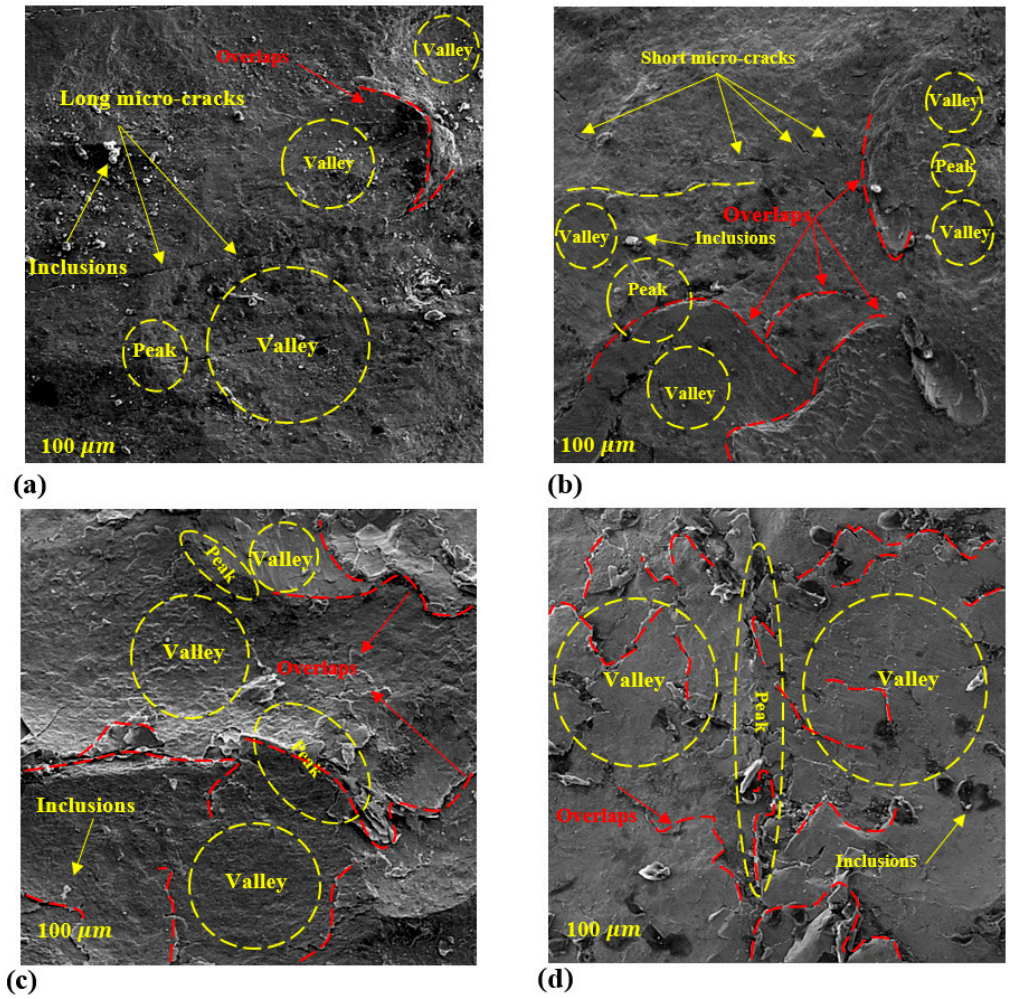

Figure 9. Scanning electron micrographs of surface morphology evolution with shot peening coverage: (**a**) 100% coverage showing uniform dimple pattern with isolated microcracks; (**b**) 400% coverage with increased dimple overlap and branched microcrack networks; (**c**) 1000% coverage exhibiting deepened dimples, 45–50% overlap density, and nano-scale bifurcated crack networks; (**d**) 1500% coverage demonstrating saturation behaviour with 55–60% overlap, work-hardening stabilization, and reduced microcrack density. Scale bars: 50 µm.

At 1500% coverage (Figure 9d), saturation behaviour emerges [2,8]. While overlap density reaches 55–60%, roughness ($R_a = 6.15$ µm) shows only 5.6% increase over 1000% coverage. This stems from work-hardening saturation (surface hardness = 343 HV) and constrained plastic flow, where subsequent impacts primarily redistribute material rather than deepen features. Microcrack density reduces by approximately 20% as surface nanocrystallization completes, though peak-to-valley amplitude remains stable [8]. The data presented in Table 7 indicate that the observed trend is consistent with the fatigue and residual-stress results.

Hardness measurements reveal that both surface coverage and Almen intensity significantly influence work-hardening behaviour [31]. Surface coverage exerts a more pronounced effect on core hardness evolution. Surface hardness escalates from 199 HV (as-received) to 343 HV (1500% coverage), representing a 72% improvement. The most substantial increase occurs between 1000% and 1500% coverage (5.2% increment), suggesting intensified work-hardening or potential microstructural refinement. Core hardness remains

nearly stable (200–223 HV), confirming that the treatment primarily affects the near-surface region with limited penetration depth.

Table 7. Surface and core hardness by shot peening coverage.

Specimen	Surface Hardness (HV)	Core Hardness (HV)
As-received	199	200
100% coverage	244	202
400% coverage	259	210
1000% coverage	326	216
1500% coverage	343	223

To assess the possibility of microcrack formation or detachment of the strengthened layer under severe shot peening, cross-sectional metallographic observations were examined for the highest coverage condition. The micrographs confirm the integrity of the near-surface strengthened layer and allow direct evaluation of any localized damage induced by over-peening.

Figure 10 presents a comparative analysis of coverage effects on hardness and surface roughness characteristics. The bar chart (Figure 10a) demonstrates that increasing coverage to 1500% yields an 11.5% enhancement in core hardness relative to the as-received condition, while surface hardness exhibits a more substantial 72% improvement. Marginal gains of only 5.2% (surface) and 3.2% (core) are observed when increasing coverage from 1000% to 1500%, indicating saturation as the material approaches maximum work-hardening capacity. Additional impacts primarily redistribute the microstructure rather than induce further refinement [31].

Surface roughness parameters R_a and R_q show minimal variation between 1000% and 1500% coverage, suggesting that the overlapping dimple network limits additional roughness development. Both parameters measure vertical deviations from the mean surface, with more sensitive to extreme peaks and valleys. Their parallel trend (Figure 10b) indicates that increased coverage from 1000% to 1500% creates uniform plastic deformation rather than isolated extreme features. The minimal divergence suggests impacts are evenly distributed, preventing outlier formation.

The most significant coverage-dependent change appears in total roughness (R_t), which increases by 2975% at 1500% coverage compared to as-received samples, with a 165% difference between 1000% and 1500% coverage. measures the peak-to-valley height of the single largest irregularity. The surge at 1500% coverage occurs because: (i) cumulative impacts deepen individual dimples; (ii) overlapping impacts smooth intermediate features, leaving fewer but more extreme outliers; (iii) stochastic multi-impact events create localized "big-dimples" while homogenizing surrounding areas; and (iv) plasticity exhaustion causes new impacts to preferentially strike existing dimples rather than generate fresh features, evidenced by >85% overlap ratio at 1500% coverage.

The hardness progression follows expected trends, with surface layers experiencing greater hardening (72%) than core regions due to strain gradient effects. Decreasing marginal gains at higher coverages reflect the natural limitations of dislocation-based strengthening mechanisms in the material.

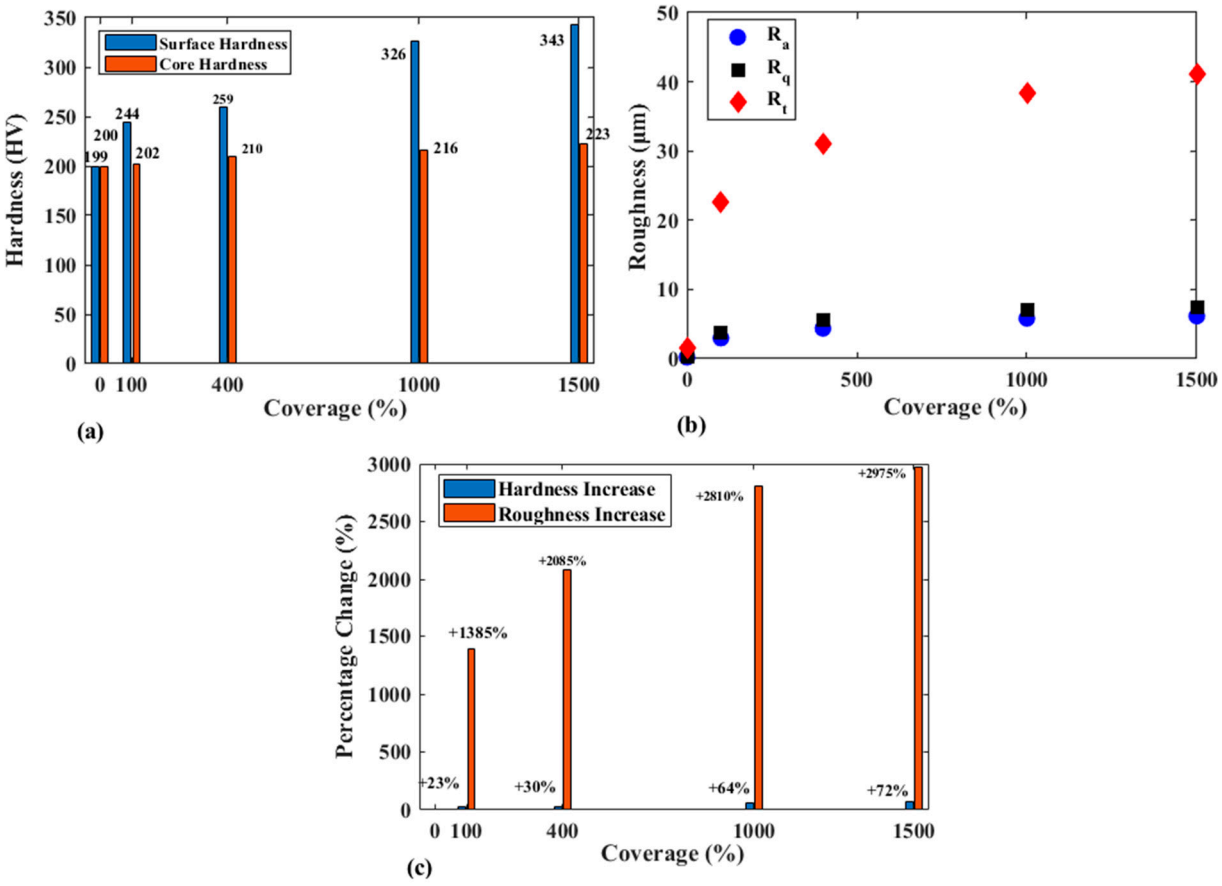

Figure 10. Coverage-dependent surface property evolution: (**a**) surface and core hardness versus shot peening coverage, showing 72% surface hardening and saturation effects above 1000% coverage; (**b**) surface roughness parameters (R_a, R_q and R_t) versus coverage, illustrating parallel $R_a - R_q$ trends and extreme R_t amplification at 1500% coverage; (**c**) changes of hardness and roughness via shot peening coverage.

3.1. Residual Stress Measurement

3.1.1. Validation of Randomized Shot Peening Using FE-Model

In this section, residual stresses were determined using numerical methods. The simulation procedure was first validated against the randomized shot peening methodology for AISI 1050 steel [18], as shown in Figure 11. Comparison between experimental results [18] and FEM simulations reveals both alignment and notable differences in residual stress profiles. Experimental measurements from Maleki et al. [18] show broader stress distributions with maximum compressive stresses of −268.9 MPa to −300.9 MPa and deeper transition depths (480–600 μm). In contrast, FEM curves predict sharper stress concentrations (−272.7 MPa for 100% coverage and −300.1 MPa for 1500% coverage) with shallower transitions (246.2 μm and 378.5 μm, respectively).

This discrepancy arises from the FEM's idealized material model, which neglects real-world factors present in experimental samples, including surface roughness, microstructural heterogeneity, and constitutive model limitations. The FEM's superior resolution of localized plastic deformation effects near the surface enables more precise capture of peak stresses, whereas experimental data reflect averaged measurements across imperfectly homogeneous material zones. However, the FEM underestimates stress penetration depth, possibly due to insufficient modelling of strain gradient effects and RVE simplification as a flat surface. Despite these differences, both datasets consistently demonstrate that higher coverage (1500%) enhances compressive stress magnitude and depth compared to standard

100% peening. The overall agreement in stress trends validates the FEM's utility for process optimization, while the deviations highlight the need for incorporating additional physical parameters to bridge the gap between simulation and experimental reality.

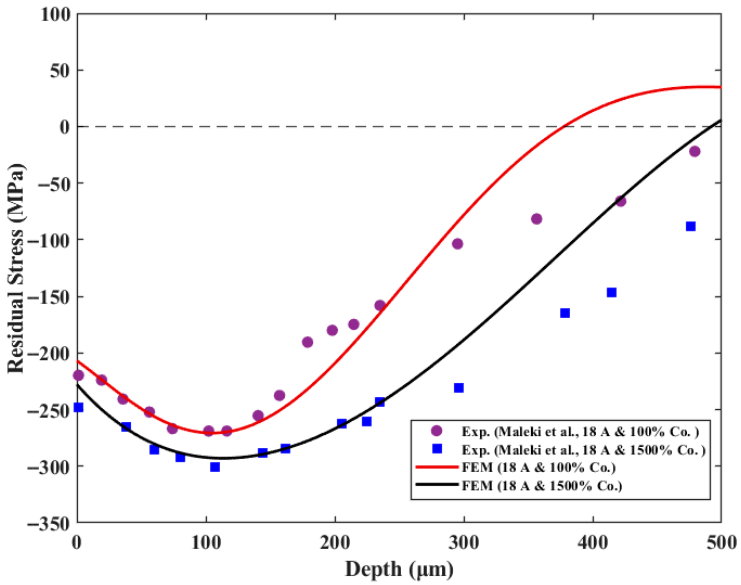

Figure 11. Validation of FE-model predictions against experimental residual stress data for AISI 1050 steel [18]: comparison of through-thickness residual stress profiles at 100% coverage and 1500% coverage, showing compressive stress magnitude, penetration depth, and transition to tensile stress. Experimental data from Maleki et al. [18]; FEM predictions from the present methodology.

3.1.2. Residual Stress Evolution with Shot Peening Coverage

The contour plots in Figure 12 visualize the spatial distribution of residual stress components (S11) within the simulated volume. These maps provide a qualitative comparison of stress arrangements across the treated region and surrounding material, but do not directly yield depth-resolved profiles at specific subsurface locations. To obtain quantitative residual stress profiles as a function of depth, the FE-Cell method [10,11] was employed to extract stress values from defined planes within the representative volume.

The residual stress contours reveal clear evolution in both magnitude and spatial uniformity with increasing coverage (Figure 12). At 100% coverage (Figure 12a), the field is distinctly heterogeneous, with compressive stresses ranging from approximately −105 MPa to −190 MPa. At 400% coverage (Figure 12b), the compressive domain extends and achieves greater continuity; the minimum compressive level intensifies to approximately −1372 MPa, indicating substantially strengthened compression compared to 100% coverage. At 1000% coverage (Figure 12c), the compressive field becomes more developed and widespread, with the minimum extending to approximately −1578 MPa and maximum tensile stress of 237.5 MPa, representing the strongest beneficial compressive capacity among non-over-peened conditions and demonstrating overlap-driven homogenization.

In contrast, 1500% coverage (Figure 12d) exhibits qualitatively different behaviour. While the compressive extreme increases further (minimum approximately −1757 MPa), the simultaneous appearance of large tensile excursions (maximum +1266 MPa) alongside severe surface distortion indicates over-peening. Excessive repeated impacts lead to stress redistribution, amplified local gradients, and tensile "hotspots" rather than uniform beneficial compressive field strengthening.

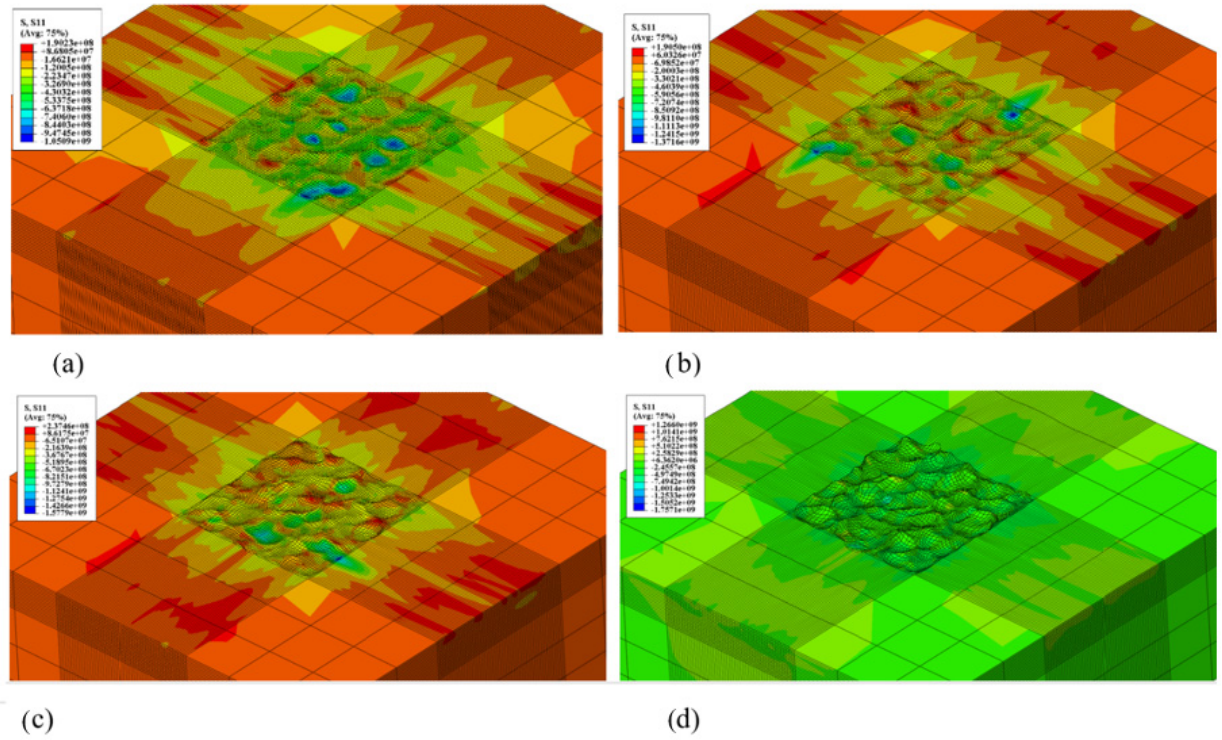

Figure 12. Residual stress contour maps (S11 component) showing coverage-dependent evolution: (**a**) 100% coverage—heterogeneous compressive field (−105 to −190 MPa) with limited overlap; (**b**) 400% coverage—extended compressive domain (−1372 MPa minimum) with improved continuity; (**c**) 1000% coverage—developed compressive field (−1578 MPa minimum, 237.5 MPa maximum tensile) representing optimal severe shot peening; (**d**) 1500% coverage—over-peening regime with maximum compression (−1757 MPa) but detrimental tensile hotspots (+1266 MPa) and severe surface distortion. Colour scale: MPa. Note: Contour extrema represent local peak stresses at individual impact sites; Figure 13 shows FE-Cell averaged profiles (Equations (2) and (3)) for fatigue correlation.

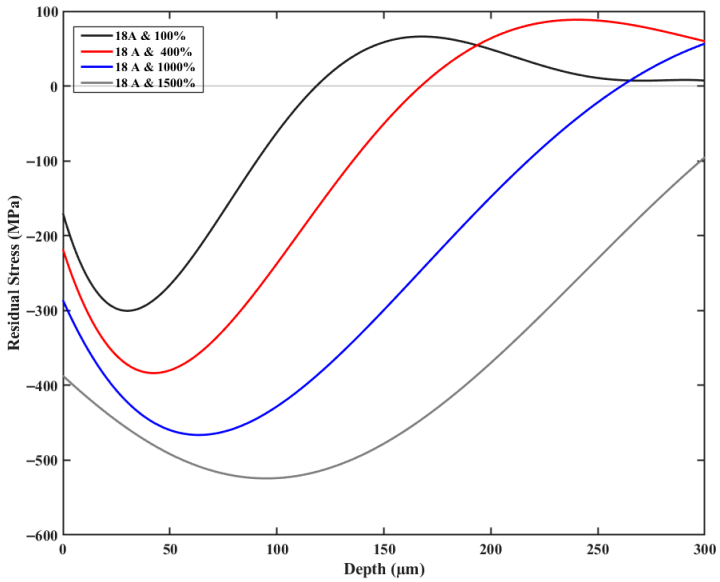

Figure 13. Through-thickness residual stress profiles by coverage level, extracted using FE-Cell method: 100% coverage (−294 MPa at 30 μm, tensile transition at 141 μm); 400% coverage (−380 MPa at 40 μm); 1000% coverage (−460 MPa at 60 μm, optimal deep compressive layer); 1500% coverage (−530 MPa at 90 μm, saturation behaviour with persistent compression to 300 μm). The shaded region indicates compressive stress; the dashed line marks zero stress.

The near-surface residual stress depth profiles (Figure 13) corroborate these coverage-dependent trends. All conditions generate compressive residual stress at the surface, followed by a subsurface compressive minimum and gradual relaxation with depth. At 100% coverage, the profile reaches −294 MPa at approximately 30 μm depth, transitioning to tensile stress beyond 141 μm. At 400% coverage, the compressive minimum deepens to −380 MPa at approximately 40 μm, with the compressive zone persisting to greater depth before tensile rebound. At 1000% coverage, the compressive state strengthens to −460 MPa at approximately 60 μm, with delayed recovery toward near-zero stress, demonstrating a substantially thickened plastically affected layer.

Importantly, the 1500% coverage profile does not represent a simple continuation of beneficial trends. Although the compressive minimum reaches −530 MPa at approximately 90 μm, saturation and redistribution behaviour are evident: residual stress remains markedly compressive (−100 MPa) even at 300 μm, without the clearer near-surface tensile rebound observed at lower coverages. This behaviour is characteristic of over-peening, where excessive plastic deformation and surface damage promote stress redistribution, meaning further coverage increases do not translate into proportionally improved, uniformly beneficial compressive residual stresses.

The contour plot in Figure 12 shows the full S11 residual stress field from the FE simulation, where local peak compressive stresses (e.g., −1372 MPa, −1578 MPa) exceed the material yield strength due to dynamic strain-rate effects and localized plastic deformation at individual shot impact sites. These represent instantaneous extrema rather than equilibrated residual stresses. In contrast, Figure 13 presents depth profiles extracted via the FE-Cell methodology (Section 2.4, Equations (2) and (3)), where residual stresses are averaged across nodal elements on discrete Γ_k planes within the representative surface cell. This averaging process yields smooth, representative values (−294 MPa at 100% coverage to −530 MPa at 1500% coverage) that correlate directly with the observed fatigue life trends. The extraction procedure follows these steps: (1) definition of a $1 \times 1 \times h_c$ mm^3 representative cell on the treated surface; (2) subdivision into depth planes Γ_k; (3) nodal averaging $\sigma_{\Gamma_n}^{ave}(y_m) = \frac{\sum \sigma_x^i}{\sum N_i}$; and (4) plotting versus depth from the surface. This approach provides statistically robust profiles for fatigue correlation, while the contour extrema in Figure 12 illustrate the full spatial variability of the stress field.

3.2. SEM and Fracture Surface Analysis

Figure 14 compares fracture surfaces of specimens tested at 44 MPa after conventional shot peening (100% coverage), severe shot peening (400% and 1000%), and over-shot peening (1500%). Each column presents the macroscopic fracture surface at the top, with progressively higher magnifications below.

For conventional shot peening (100%), the macroscopic view (Figure 14a) reveals a relatively large fast-fracture zone and comparatively small fatigue crack-growth region, with few, widely spaced beach marks. This correlates with the shortest fatigue life in this series (N_f = 28,300 cycles). At higher magnification, long, open microcracks run parallel to the peened surface, following slip bands and inclusion sites. The dimpled overload zone is ductile but contains several large cavities, indicating crack nucleation at limited dominant surface defects with rapid propagation once the shallow compressive layer is penetrated. This behaviour is typical of conventional peening, where compressive residual stresses are confined to a relatively thin layer and surface deformation is moderate [2].

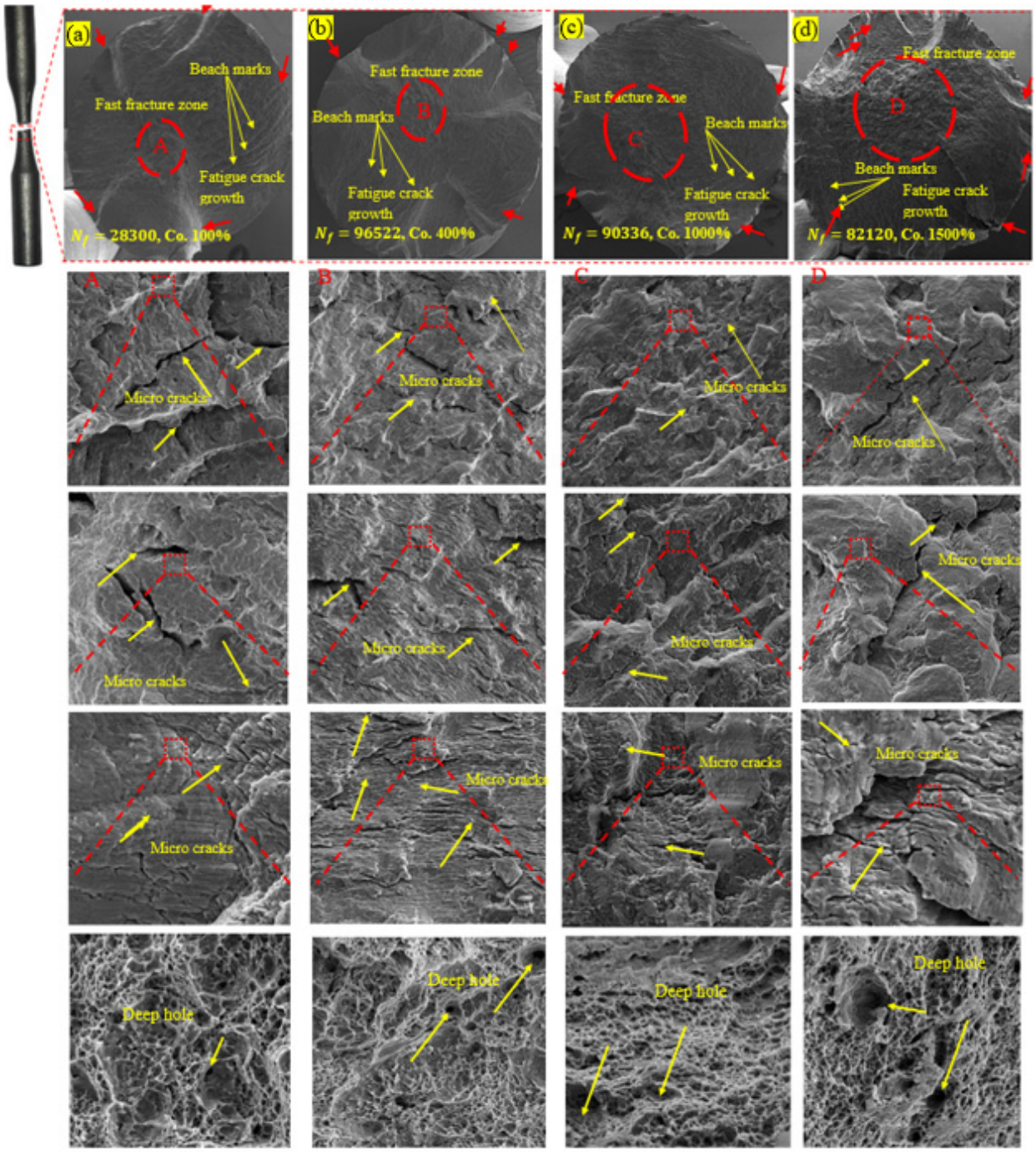

Figure 14. Fracture surface morphology evolution with shot peening coverage at 44 MPa stress level: (**a**) 100% coverage—conventional peening with shallow compressive layer, large fast-fracture zone, and limited fatigue region (N_f = 28,300 cycles); (**b**) 400% coverage—optimal severe peening with extensive fatigue crack-growth region, dense beach marks, and tortuous crack paths (N_f = 96,522 cycles); (**c**) 1000% coverage—deep compressive field with increased microcrack density, and slight life reduction (N_f = 90,336 cycles); (**d**) 1500% coverage—over-peening with expanded fast-fracture zone, stratified surface, deep voids, and damage-saturated layer (N_f = 82,120 cycles). Arrows indicate crack propagation direction; dashed lines mark compressive layer depth.

In the severe shot peening regime (400% and 1000%), morphology changes markedly. At 400% coverage (Figure 14b), the fatigue crack-growth region occupies most of the section, with dense, well-defined beach marks reflecting long, stable crack propagation and the highest fatigue life (N_f = 96,522 cycles). Intermediate magnification reveals a finely

corrugated surface with short, branched microcracks located mainly at overlapping dimple intersections. The final fracture zone shows uniform, fine dimples with only occasional deep holes, indicating a thick, work-hardened but still ductile surface layer where crack paths are highly tortuous and repeatedly deflected—consistent with deeper, more homogeneous compressive residual stresses predicted by the FE-Cell model (−380 MPa) and earlier reports on severe shot peening in steels [2,7].

At 1000% coverage (Figure 14c), the macroscopic fracture surface still exhibits an extensive fatigue region and pronounced beach marks, though the fast-fracture zone slightly enlarges and life decreases (N_f = 90,336 cycles). SEM images reveal a denser microcrack network and stepped, lamellar features within the peened layer, with high dimple overlap. FE-Cell analysis indicates this condition generates a stronger, deeper compressive field (−460 MPa, transition depth = 266 μm), implying that the slight life reduction is not stress-related but originates from increased microstructural defect density acting as additional crack-initiation sites.

The over-peened specimen (1500%) shows the most damaged morphology. In Figure 14d, the fast-fracture zone expands, and the fatigue region contracts, consistent with further life reduction (N_f = 82,120 cycles). High-magnification images reveal a heavily stratified, folded surface with numerous microcracks along interlayer boundaries and around large dimples. Deep, crater-like voids dominate the overload region, indicating local decohesion and spalling of the over-worked surface. Although FE-Cell simulations predict the highest compressive stress and the deepest affected layer at this coverage (σ_{max} = −530 MPa), SEM clearly shows a damage-saturated, locally brittle surface. This mirrors previous observations that extreme coverage or kinetic energy degrades fatigue performance by introducing microcracks, surface tearing, and sub-surface voids despite extended compressive residual stress profiles [2,32,33].

Taken together, Figure 14 demonstrates rational progression: conventional shot peening produces limited strengthening due to shallow compressive layers; severe shot peening (400–1000%) optimally balances deep compressive field, high hardness, and controlled surface morphology for longest fatigue lives; further intensification to 1000–1500% at 45 MPa stress level drives the system into over-peening regime where microcracking, delamination, and deep void formation outweigh benefits of additional compressive stress.

4. Conclusions

This investigation systematically evaluated the effects of conventional and severe shot peening on AISI 4140 steel fatigue performance across coverages of 100%, 400%, 1000%, and 1500% at a fixed 18A Almen intensity under rotating-bending loading. A combined experimental and numerical approach integrated fatigue life assessment with FE-Cell-based residual stress analysis and surface characterization to establish optimal processing parameters for industrial application.

Fatigue life improvement exhibited non-monotonic dependence on coverage, with optimal performance at 1000% coverage under 37 MPa (797% increase versus as-received). This optimal coverage shifted with applied stress amplitude: 1500% excelled at 40.5 MPa (538% improvement), while 400% was optimal at 44 MPa (405% improvement), indicating reduced tolerance to surface degradation as stress levels increase. Beyond these thresholds, excessive coverage induced over-peening effects: 33% life reduction at 1500% under 37 MPa and 15% decrease at 1500% versus 400% under 44 MPa, attributable to microcrack nucleation and surface damage saturation.

Surface characterization revealed systematic evolution of roughness and hardness with increasing coverage, though saturation effects emerged at extreme levels. Surface roughness parameters R_a, R_q, and R_t increased from 0.20 μm, 0.25 μm, and 1.50 μm to 6.15 μm, 7.50 μm, and 41.20 μm at 1500% coverage, while surface hardness demonstrated work-hardening enhancement from 199 HV to 343 HV with stable core hardness at 200–223 HV.

The FE-Cell methodology successfully quantified coverage-dependent residual stress evolution. Maximum compressive stress increased from −294 MPa at 100% coverage (shallow subsurface, tensile transition at 141 μm) to −503 MPa at 1500% coverage (compressive zone exceeding 300 μm). However, the 1500% condition exhibited characteristic overpeening behaviour—stress redistribution and elevated near-surface tensile excursions—that offset the benefits of deeper compressive stress penetration.

The optimal coverage window of 400–1000% identified for AISI 4140 steel under rotating-bending fatigue is expected to provide useful guidance for other high-strength, medium-carbon alloys (e.g., AISI 4340, 42CrMo) subjected to similar cyclic bending or torsional loading in rotating components. The stress-dependent shift in optimal coverage (lower coverage optimal at high stress, higher coverage optimal at low stress) likely represents a general phenomenon governed by the interplay between compressive residual stress depth, surface integrity, and applied stress amplitude. While material-specific calibration remains necessary, the present findings establish a robust baseline for severe shot peening optimization across a range of engineering alloys and service environments.

These results establish that severe shot peening at 400–1000% coverage provides the most robust processing window for AISI 4140 steel at 18A Almen intensity, achieving deep compressive residual stresses with controlled surface integrity and maximum fatigue life gains. Identification of coverage-dependent optimal stress regimes offers practical guidance for industrial implementation, enabling tailored surface treatment selection based on anticipated service loading conditions.

Author Contributions: Conceptualization, M.F., K.R.K. and M.C.; methodology, M.F., K.R.K. and M.C.; software, M.F.; validation, M.F. and K.R.K.; formal analysis, M.F., K.R.K., R.N., H.S. and H.D.; investigation, M.F., R.N., H.S. and H.D.; resources, K.R.K.; data curation, M.F. and K.R.K.; writing—original draft preparation, M.F., R.N., H.S., M.C. and H.D.; writing—review and editing, K.R.K.; visualization, M.F. and K.R.K.; supervision, K.R.K.; project administration, M.F.; funding acquisition, M.F., K.R.K. and M.C.; All authors have read and agreed to the published version of the manuscript.

Funding: There is not funding for this research.

Data Availability Statement: The original contributions presented in this study are included in the article. Further inquiries can be directed to the corresponding author.

Acknowledgments: This paper was supported by the RUDN University Strategic Academic Leadership Program.

Conflicts of Interest: The authors declare no conflict of interest.

References

1. Wu, K.; Li, K.; Hao, L.; Tang, J.; Jin, X.; Yang, J. Effects of shot peening intensity and coverage on the fatigue life and fracture characteristics of DZ125 alloy at room and high temperatures. *Eng. Fail. Anal.* **2025**, *167*, 108955. [CrossRef]
2. Maleki, E.; Farrahi, G.H.; Kashyzadeh, K.R.; Unal, O.; Gugaliano, M.; Bagherifard, S. Effects of conventional and severe shot peening on residual stress and fatigue strength of steel AISI 1060 and residual stress relaxation due to fatigue loading: Experimental and numerical simulation. *Met. Mater. Int.* **2021**, *27*, 2575–2591. [CrossRef]
3. Hadad, M.; Darzi, J.G.; Mahdianikhotbesara, A.; Makarian, J. Experimental investigation of the effect of single point dressing parameters on grinding of Mo40 hardened steel using mounted point grinding tool. *Energy Equip. Syst.* **2022**, *10*, 197–214.

4. Farrahi, G.H.; Lebrijn, J.L.; Couratin, D. Effect of shot peening on residual stress and fatigue life of a spring steel. *Fatigue Fract. Eng. Mater. Struct.* **1995**, *18*, 211–220. [CrossRef]
5. Tekeli, S. Enhancement of fatigue strength of SAE 9245 steel by shot peening. *Mater. Lett.* **2002**, *57*, 604–608. [CrossRef]
6. Karimbaev, R.; Pyun, Y.-S.; Maleki, E.; Unal, O.; Amanov, A. An improvement in fatigue behavior of AISI 4340 steel by shot peening and ultrasonic nanocrystal surface modification. *Mater. Sci. Eng. A* **2020**, *791*, 139752. [CrossRef]
7. Maleki, E.; Unal, O.; Kashyzadeh, K.R. Effects of conventional, severe, over, and re-shot peening processes on the fatigue behavior of mild carbon steel. *Surf. Coat. Technol.* **2018**, *344*, 62–74. [CrossRef]
8. Maleki, E.; Unal, O.; Kashyzadeh, K.R.; Bagherifard, S.; Guagliano, M. A systematic study on the effects of shot peening on a mild carbon steel: Microstructure, mechanical properties, and axial fatigue strength of smooth and notched specimens. *Appl. Surf. Sci. Adv.* **2021**, *4*, 100071. [CrossRef]
9. Liu, H.; Zhu, W.; Jiang, C.; Guagliano, M.; Xing, S.; Wang, L.; Ji, V.; Zhan, K. Microstructure evolution and residual stress distribution of nanostructured Mg-8Gd-3Y alloy induced by severe shot peening. *Surf. Coat. Technol.* **2020**, *404*, 126465. [CrossRef]
10. Forouzanmehr, M.; Kashyzadeh, K.R.; Laad, M. Effects of ring indentation, punching, and shot peening treatments on fatigue crack retardation considering modified J-integrals: A comparative study. *Eng. Fail. Anal.* **2025**, *170*, 109282. [CrossRef]
11. Kashyzadeh, K.R.; Forouzanmehr, M.; Mahmoudi, A.H.; Farrahi, G.H. Novel Finite Element-Cell based Methodology for Evaluating Residual Stress Distribution Caused by Punching Process in Plane Crack Problems. *Int. J. Eng.* **2026**, *39*, 547–560. [CrossRef]
12. ASTM Steel. SAE 4140 Steel: Comprehensive Guide and Insights. 2023. Available online: https://www.astmsteel.com/steel-knowledge/sae-4140-steel/ (accessed on 4 March 2026).
13. Ryerson. What is 4140 Steel?—Properties, Applications and Benefits. 2024. Available online: https://www.ryerson.com/metal-resources/metal-market-intelligence/grade-anatomy-4140 (accessed on 4 March 2026).
14. *International Standard ISO 1143*; Mettalic Materials—Rotating Bar Bending Fatigue Test. 3rd ed. ISO: Geneva, Switzerland, 2021.
15. Johnson, D.R.; Gruninger, M.F. Practical Examples and Implications of Almen Strip Physics. *Shot Peen.* **2024**, *38*.
16. Bag, A.; Lévesque, M.; Brochu, M. Effect of shot peening on short crack propagation in 300 M steel. *Int. J. Fatigue* **2020**, *131*, 105346. [CrossRef]
17. Brick, C.M.; Chan, E.R.; Glotzer, S.C.; Marchal, J.C.; Martin, D.C.; Laine, R.M. Self-Lubricating Nano-Ball-Bearings. *Adv. Mater.* **2007**, *19*, 82–86. [CrossRef]
18. Unal, O.; Maleki, E.; Karademir, I.; Husem, F.; Efe, Y.; Das, T. Effects of conventional shot peening, severe shot peening, re-shot peening and precised grinding operations on fatigue performance of AISI 1050 railway axle steel. *Int. J. Fatigue* **2022**, *155*, 106613. [CrossRef]
19. Yang, H.; Zhang, Z.; Tan, C.; Ito, M.; Pan, P.; Wang, X. Rotating bending fatigue microscopic fracture characteristics and life prediction of 7075-T7351 Al alloy. *Metals* **2018**, *8*, 210. [CrossRef]
20. Milovanović, V.; Gicić, M.; Zivkovic, M.; Živković, J.; Dunić, V. Development of an software application for post-processing of experimentally obtained fatigue properties of metallic materials. In *Book of Abstracts*; Gutenberg Press: Mainz, Germany, 2023.
21. Sweat, L.H.; Johnson, K.B. The effects of fine-scale substratum roughness on diatom community structure in estuarine biofilms. *Biofouling* **2013**, *29*, 879–890. [CrossRef] [PubMed]
22. Todhunter, L.; Leach, R.; Lawes, S.; Blateyron, F. Industrial survey of ISO surface texture parameters. *CIRP J. Manuf. Sci. Technol.* **2017**, *19*, 84–92. [CrossRef]
23. Qin, S.; Saewe, J.; Kunz, J.; Herzog, S.; Kaletsch, A.; Schleifenbaum, J.H.; Broeckmann, C. Influence of preheating temperature on microstructure evolution and hardness of high-speed steel AISI M50 processed by laser powder bed fusion. *Steel Res. Int.* **2023**, *94*, 2200784. [CrossRef]
24. *ASTM E92-17*; Standard Test Methods for Vickers Hardness and Knoop Hardness of Metallic Materials; ASTM Standards. ASTM International: West Conshohocken, PA, USA, 2017.
25. Soldani, X.; Moufki, A.; Molinari, A.; Budak, E.; Özlü, E. High speed machining of AISI 1050 steel: Modelling and experimental. *Int. J. Mater. Form.* **2008**, *1*, 1439–1441. [CrossRef]
26. Tekkaya, B.; Meurer, M.; Münstermann, S. Modelling of grain size evolution with different approaches via FEM when hard machining of AISI 4140. *Metals* **2020**, *10*, 1296. [CrossRef]
27. Bagherifard, S.; Ghelichi, R.; Guagliano, M. A numerical model of severe shot peening (SSP) to predict the generation of a nanostructured surface layer of material. *Surf. Coat. Technol.* **2010**, *204*, 4081–4090. [CrossRef]
28. *J2277*; Shot Peening Coverage Determination. Developed by Surface Enhancement. SAE International: Warrendale, PA, USA, 2003; Volume 660.
29. DKirk, M.; Abyaneh, M.Y. Theoretical basis of shot peening coverage control. *Shot Peen.* **1995**, *9*, 28–30.
30. He, W.; Yan, C.; Gorbachev, S.; Kuzin, V. Numerical simulation of shot peening process for AISI 4340 steel using random balls method. *Trans. Indian Inst. Met.* **2023**, *76*, 2601–2614. [CrossRef]

31. Gao, H.; Lin, M.; Guo, J.; Yang, L.; Wu, Q.; Ran, Z.; Xue, N. A simulation modeling methodology considering random multiple shots for shot peening process. *Rev. Adv. Mater. Sci.* **2023**, *62*, 20220304. [CrossRef]
32. Ghasemi, A.; Hassani-Gangaraj, S.M.; Mahmoudi, A.H.; Farrahi, G.H.; Guagliano, M. Shot peening coverage effect on residual stress profile by FE random impact analysis. *Surf. Eng.* **2016**, *32*, 861–870. [CrossRef]
33. Gangaraj, S.; Guagliano, M.; Farrahi, G. An approach to relate shot peening finite element simulation to the actual coverage. *Surf. Coat. Technol.* **2014**, *243*, 39–45. [CrossRef]